Inferring sediment transfers and functional connectivity of rivers from repeat topographic surveys

Calle, Mikel[1*] (m.calle@mncn.csic.es)

Calle, Javier[2] (jcalle64@alumno.uned.es)

Alho, Petteri[3] (mipeal@utu.fi)

Benito, Gerardo.[1] (benito@mncn.csic.es)

[1] National Museum of Natural Sciences, Spanish Research Council (CSIC), Madrid, Calle de Serrano 115 bis, 28006 Madrid, Spain

[2] National Distance Education University (UNED), Madrid, Calle de Bravo Murillo, 38, 28015 Madrid, Spain

[3] Department of Geography and Geology, University of Turku, Turku, 20014 Turun yliopisto, Finland

Data availability statement: Pre-process, processed and post-processed data are shared in the supplementary section.

Running Head: Morphological dynamics, sediment transfer and connectivity in rivers

Key Points:

An ephemeral gravel-bed river was monitored to evaluate morphological changes, sediment transfers and functional sediment connectivity caused by flood events.

Repeat photogrammetric flights provided quantification of morphological change and sediment budgets.

The proposed systematic method for river segmentation allowed transforming the results of the DEM of difference into sediment transport distances and precise quantification of a river's functional connectivity.

Relatively large volume changes, long sediment transport distances and values of connectivity far from equilibrium ($C_{v\text{-}strip} \neq 1$) were interpreted as unbalanced reach morpho-sedimentary dynamics commonly associated with gravel extraction sites.

Abstract

High-resolution topographic models have revolutionized monitoring of river changes by comparing sequential river topographic surveys, i.e. change detection. Nevertheless, much more may be obtained from this innovative quantification of changes. In this paper, we enhance the interpretation of geomorphic processes by presenting a new method for understanding of sources and sinks of sediment, river sediment transfers and functional sediment connectivity.

Repeat digital elevation models (DEMs) obtained by photogrammetry were used to quantify topographic change after two floods by creating DEM of difference (DoD) of a 6.5 km-long reach of Rambla de la Viuda stream, an ephemeral gravel-bed river in eastern Spain. The proposed method involved dividing the channel

into 10 m-long longitudinal strips that were used to sistematically draw boundaries between the erosional and depositional areas of the DoD. The analysis objectively: i) drew a series of erosional and depositional segments, from 120 to 1360 m in length, ii) estimated ranges of source-to-storage sediment transport distances, 320-670 m in the upstream and middle reaches and up to 2030 m in the lower reach, and iii) obtained values of functional connectivity, i.e. the ratio between the sediment exported (erosion) and retained (deposition), ranging from 10^{3} and 10^{-3}. The variability in these three parameters along the river was found to be related to the level of channel disturbance by in-stream mining during the 1990s and 2000s. Additionally, this method indicates that that main process responsible for self-adjustment of the present morphosedimentary conditions is intra-reach erosion of banks and channel beds. Thus, this study proposes a new methodology to characterize morphological change, sediment transfer and connectivity that may serve as environmental indicators of the hydromorphological integrity of rivers with potential application to the European Water Framework Directive.

Key words: Functional connectivity; change detection; SfM-MVS; transport distance; hydromorphological assessment

Twitter publicizing: A new approach to estimate sediment transfer and functional sediment connectivity in river corridors is applied to traditional change detection methods (DoD).

1 Introduction

The study of morphological response of river channels to hydrological events and human induced impacts requires a proper understanding of how sediment transfers along river courses. This is of special interest today given that rivers are suffering morphological changes, some of them irreversible, without a complete understand of the rate and consequence of such changes. It is known that the relation between discharge, sediment availability and bedload transport controls river morphology, and therefore ecology (Lisle et al., 2001; Brooks and Brierley, 2004; Hodge et al., 2009a). However, a precise determination of these relations are strongly limited by the difficulty of recording spatio-temporal changes on river surface morphology and bedload transport (Hodge et al., 2009b).

Recent development in high precision and high-resolution topographic reconstruction techniques and its application to riverine environments opened a variety of opportunities, from extensive grain size estimations (Hodge et al., 2009a; Hodge et al., 2009b; Wang et al., 2013), high-resolution topographic mapping (Alho et al., 2009; Javernick et al., 2014), to change detection (Eltner et al., 2017; Calle et al., 2018). Accordingly, the number of high quality topographic data and objective quantifications of river changes increased worldwide (Brasington et al., 2012; Flener et al., 2013; among others). The development of topographic methods, with increase resolution and survey frequency offers an unprecedented opportunity to quantify the relation between morphologic changes and the actual sediment transfers. This is known as the 'inverse approach' or 'morphological approach', i.e. an inverse solution to

93 estimating sediment transport through sediment budgeting (see review in Vericat
94 et al., 2017). In this process, repeated high-resolution digital elevation models is
95 key to infer sediment transfers and transport paths (Heckmann and Vericat,
96 2018). In rivers, a similar approach has been used to estimate sediment transport
97 rates and route the sediment cell-by-cell along the channel by coupling a 2D
98 hydraulic simulation (Antoniazza et al., 2019).

99 Implicitly, quantifying sediment transfer along a river reflects in a certain way the
100 capacity of a reach to retain or flush sediment. This involve the rate at which water
101 and sediment move downstream, a quality known as sediment 'connectivity'
102 (Wohl, 2017). The concept of connectivity is still relatively unclear, and its
103 definition and use in the contexts of water and sediment dynamics have been the
104 subject of longstanding controversy (Kondolf et al., 2006; Bracken and Croke,
105 2007; Fryirs et al., 2007; Huang and Ding, 2016; Wohl, 2017; Heckmann and
106 Vericat, 2018). Studies on this topic indicate that connectivity is a variable state
107 in a system (Heckmann and Vericat, 2018) which can be linked to the spatial
108 configuration of sediment pathways and reflects the "intrinsic potential" of
109 landscape elements to be connected, i.e. structural connectivity (Cavalli et al.,
110 2013). The term connectivity may also refers to the system dynamics, the actual
111 sediment transfer between the components of a geomorphic system at certain
112 time and spatial scale i.e. functional connectivity (Bracken et al., 2015). In
113 practice, some studies have determined structural connectivity based on physical
114 parameters along the fluvial system (e.g. Crema and Cavalli, 2018), but only a
115 few provided semi-quantitative indicators of functional connectivity (Hooke, 2003;
116 Lehotský et al., 2018). Recently, Heckmann and Vericat (2018) succeeded in
117 precisely quantifying sediment volumes that have been deposited, temporarily

stored or flushed using repeated DEMs (digital elevation models) on a steeply sloping lateral moraine. Quantification of these transfers or retentions into the same downslope pathway (sediment delivery ratios), were suggested to be a measure of functional sediment connectivity (Heckmann and Vericat, 2018). Similar approach, adapted to long river segments, can be used to objectively estimate the actual sediment transfer through river reaches. Thus, the volume of particles entrained from or retained within a river reach can be considered a measure of functional sediment connectivity, or rather disconnectivity (Fryirs et al., 2007; Bracken et al., 2015).

Therefore, this paper aims at applying repeated high-resolution topographic models to: (1) quantify sediment retention and entrainment at different scales within the river corridor based on data obtained from repeat topographic models (DEMs); (2) develop a method for further analysis of topographic data that could: i) objectively determine the spatial pattern of morphological change; ii) provide insights into the transport distances of bedload particles during floods; and iii) assess whether transport distances and retention volumes can be used as a quantitative measure of functional river connectivity. Finally, it also aims to (3) discuss its applicability for assessing a river's environmental state in ephemeral rivers considering, with the potential of being used as a tool for its hydromorphological evaluation under the European Water Framework Directive.

2 Study Site

The study area comprises a 6.5 km reach of the Rambla de la Viuda River, located in Castellón province (eastern Spain), with a total catchment area of 1523

141 km^2 (Figure 1). This river reach is entrenched in Cretaceous limestone bedrock
142 related to a horst area of the Maestrat graben system (25-3 M.a.) (Anadón and
143 Moissenet, 1996; Simón et al., 2013). During the Quaternary era, the last
144 reactivation of this fault system simultaneously interacted with the fluvial
145 landscape generating the present alluvial valley bottoms (Simón et al., 2013). The
146 study reach has an average gradient of 0.0059 and a width of 30 to 125 m. Since
147 the 1960s, intensive in-stream gravel mining has reduced the sediment
148 availability in this ephemeral stream, with a subsequent recovery period from
149 2000 until the present (Calle et al., 2017). Generalized bed degradation and the
150 formation of micro-terraces (1-2 m) are also associated with gravel mining. During
151 the study period, the sediment size in active areas was 22.6 mm (D50), 32.5 mm
152 (D84) and 41.4 mm (D90) according to methods described in Section 3.3.

153 The Rambla de la Viuda River has an ephemeral hydrology dominated by flash
154 flooding. Only high-intensity rains (>70 mm/day) are able to produce runoff in the
155 study area (Camarasa-Belmonte and Segura-Beltrán, 2001), and are typically
156 concentrated in winter and autumn. Autumn is the period of most intense rainfall,
157 usually due to atmospheric situations with cut-off lows leading to the formation of
158 mesoscale convective systems. The average number of rainfall events producing
159 streamflow over the period 1960-2000 was 2-3 per year, with an annual average
160 stream flow duration of 30 days (Camarasa-Belmonte and Segura-Beltrán, 2001).
161 Major floods are an important component of this irregular hydrological regime,
162 with some peak flows exceeding 600 m^3s^{-1} in 1920, 1962, 1969 and 2000
163 (Machado et al., 2017).

3 Methods

3.1 DEMs

This study compares changes in consecutive digital elevation models (DEMs) derived from photogrammetric campaigns. Structure from Motion combined with Multi View Stereo (SfM-MVS) reconstruction algorithms solved cost and time issues at a reasonable trade-off between measurement accuracy and resolution (Verhoeven et al., 2015; Calle et al., 2018). The literature contains good descriptions of the theoretical basis of SfM-MVD (Snavely, 2009; Brasington et al., 2012; Westoby et al., 2012), software functioning (Verhoeven, 2011; Jaud et al., 2016) and its applicability in rivers (Javernick et al., 2014). This section gives a short description of the flights and photo acquisition for obtaining DEMs, and a more detailed explanation of SfM-MVS methods and performance can be found in Calle et al. (2018).

Photogrammetric campaigns followed the same approach: low-elevation aerial photos taken from an autogyro with a hand-held camera. Photo targets (25 x 25 cm) were used for georeferencing and analysing the quality of the reconstructed topography. Around 140 targets were deployed whose centroids were measure with a Real Time Kinematics GPS (Trimble RTK 4700) with errors set below 0.02 in XY and 0.05 in Z. Two thirds of the targets were used as ground control points (GCPs) and the remaining third was used as independent check points for assessing precision and accuracy of the reconstructed surface. A summary of the flight characteristics used during the field campaigns are shown in Table 1. Detailed survey characteristics is carefully explained in Calle et al. (2018) and presented in table-format as a digital supplement (‘Detailed Survey

188 Characteristics'). Camera resolution, flight path and flight height were modified in
189 each flight to resolve the problems encountered during the campaigns (see Calle
190 et al., 2018, for further details). These flights captured the activity caused by two
191 flow events registered in March and November 2015, with a peak discharge of 98
192 m^3s^{-1} and 80 m^3s^{-1}, total volume of 32.5 hm^3 and 7.1 hm^3, and 24 and 11 days of
193 streamflow respectively.

194 Photogrammetric reconstructions were carried out in PhotoScan software
195 (version 1.2.6). Detailed information about workflow and computation
196 parameters, such alignment, processing and point cloud characteristics, are
197 given in Calle et al. (2018) and as a supplementary data (Table of PSS:
198 photogrammetric survey specifications). Change detection, DEM of difference
199 (DoD) and volume calculations were done entirely in ArcGIS. Change detection
200 and DoD were obtained by subtracting the final topography from the previous
201 topography (Wheaton et al., 2010; Alho et al., 2011; Kasvi et al., 2013; Lotsari et
202 al., 2014). Active river areas were isolated from DoD using a polygon that masked
203 the area with changes observed in the orthophotomosaics. DoD were created
204 with the same spacing as the DEMs (0.25x0.25 m), and the centroid locations of
205 the pixels coincided exactly.

206 Individual errors in the DEMs and the level of detection (LoD) of the DoD were
207 estimated to be lower than ± 0.20 m (Calle et al., 2018). The LoD considers the
208 propagation of error (2σ) of each DEM to give a general accuracy of the DoD
209 (Brasington et al., 2003; Lane et al., 2003). This means that all deposition
210 (aggradation) and erosion (incision) between 0.20 and -0.20 m have been

211 excluded from the calculations, thereby avoiding methodological error in the
212 estimation of sediment storage and entrainment (Lane et al., 2005).

213 3.2 A methodology for estimating sediment transport

214 Our methodological approach for estimating sediment transport distances is
215 based on the following assumptions: 1) the active river corridor is evenly divided
216 into longitudinal compartments ('strips') that will be used as the units for
217 calculations; 2) each strip is considered to behave homogenously in its most
218 representative process, namely erosion or deposition, although it may contain
219 features of both; 3) sediment transport is necessarily unidirectional, and sediment
220 is always assumed to displace downstream; and 4) the porosity and compaction
221 of the sediment (estimated volumes) remains constant in space and time.

222 Data pre-processing and strip division was entirely conducted with ArcGIS
223 Desktop tools. A detailed description of its application to the DEMs and DoD can
224 be found in 'Supplementary data 1'. It also includes the criteria for longitudinal
225 strip length selection, whose values may vary according to user's scope and river
226 characteristics. In this case, a value of 10 m was selected.

227 The limits between adjacent strips are defined as 'boundaries', which are the
228 vertical planes that separate strips. Five types of relationship can be described
229 between estimated sediment volumes of an upstream (V1) and a downstream
230 (V0) strip (Figure 2). Depositional boundaries (type #1) allow the estimation of
231 transport distances by assuming that the downstream deposit is mainly
232 generated by upstream erosion; a similar hypothesis to the one applied by Goff
233 and Ashmore (1994). Two different approaches can be considered to obtain a

range of transport distances (1 and 2): 1) if the total volume of sediment found downstream of the boundary is considered (Figure 3, approach 1), the sediment volume that has been eroded can be counted upstream, strip by strip, until the balance of the total downstream sediment is reached. A maximum and minimum transport distance range can then be estimated. A maximum transport distance (1a) is estimated for the net volume of each strip (deposition minus erosion). However, if only the erosive component (instead of the net component) is considered, we obtain a minimum transport distance (1b). 2) Conversely, the same can be estimated in the case of the total volume of upstream erosion. The equivalent volume that has been eroded can be counted downstream of the boundary, strip by strip, to obtain the distance from which the sediment was exported. A maximum transport distance is estimated (2a) for the net volume of each strip (deposits minus erosion). A minimum transport distance (2b) is obtained if only the deposition component of the strips is considered. In summary, the theoretical minimum and maximum transport distances bracket the range of potential particle motion, so the minimum transport calculated by cases 1a and 2a and the maximum transport calculated by 1b and 2b include all the possible transport distances without the possibility of any closer or farther displacements.

This conceptual model was implemented in the Visual Basic for Applications code, calculating the maximum and minimum distance of depositional boundaries using the data obtained from DoD. Further explanations and the actual code used can be found in Supplementary data 2.

3.3 Active sediment size and tracer analysis

Grain size distribution and movement of marked particles (tracers) were investigated to validate morphological interpretations and estimated transport ranges. Gravel-size measurements were made from 100 clasts sampled at 58 representative active bars following Wolman (1954) guidelines. Clasts were collected every 0.5 m along two parallel 25-m segments –an adequate length since the Rambla de la Viuda's present bar size is ~40 m (Calle et al., 2017)– aligned with the flow direction.

The movement of tracers was used to discuss the estimated sediment transfers. Three stations of around 50 clasts each, ranging from 22.6-128 mm, were distributed along the reach (see location in Figure 1-b). The stations were placed according to the potential behaviour of the sub-reaches. They were intended to correlate erosive, transitional and depositional sub-reaches, from upstream to downstream. Within each station, the clasts were lined up following a cross section, covering the main channel and active bars on both sides. The comparison between pre- and post-flood locations of the 153 stones was carried out with RTK-GPS measurements and then transformed into horizontal distances.

3.4 Sediment conveyance and retention as a measure of connectivity

River sediment connectivity has been defined as the capacity of a river reach to retain or deposit sediment (Hooke, 2003). A measurement of the volume of particles that has been deposited or retained along a river reach is then a

measure of bedload sediment connectivity or rather disconnectivity (Fryirs, 2013; Wester et al., 2014; Bracken et al., 2015; Wohl, 2017). Following this definition, a connectivity value per strip ($C_{v\text{-}strip}$) is calculated at each channel strip as the relation between the volume of retained sediment (deposition) and the exported sediment (erosion) at a specific event or subsequent events (1), i.e. functional sediment connectivity.

$$C_{v-strip} = \frac{Erosion}{Deposition} \quad (1)$$

This relationship implies more connectivity at strips where erosion exceeds deposition and conversely decreases as the accumulation or deposition increases in relation to erosion. Thus, a value of 1 expresses dynamic stability conditions at the channel strip, where inputs and outputs are closely matched.

4 Results

4.1 Reach-scale geomorphic changes: total mobilized volumes

The primary result of the change detection process is to quantify the river's morphodynamics (Heckmann and Vericat, 2018), which shed light on two additional aspects: i) sediment budget and net inputs/outputs, ii) the river's activity levels, and iii) the source of the mobilized sediment.

Reach scale DoD maps accounted for 166,296 m^3 of total mobilized sediment, of which 73,803 m^3 was detected as erosion and 92,493 m^3 as deposition. The net sediment input is therefore 18,690 m^3; however, this value does not represent an intuitive expression of river channel activity. For example, a net input of 0 might indicate a river reach with a balanced deposition and erosion but a high amount

of mobilized sediment. For this reason, the 'relative activity' of different geomorphic systems may be better evaluated based on the amount of total mobilized volumes per unit area in the active area of the study reach. Thus, the relative activity level per unit area is therefore proposed as a tool for future comparisons among river channels and systems. This activity value will be dependent to magnitude and frequency of the flood event and it should be carefully considered when comparing different systems or flood events.

In the following example, activity levels are estimated in different cases to view its applicability. The geomorphic activity in the Rambla de la Viuda River was 0.4 m^3/m^2; i.e. 166,296 m^3 within an active area of 417,274 m^2. In contrast to the net input, this is comparable with other rivers and regions. For instance, processes that are supposed to produce high activity levels in channels, such a lake-breakout in New Zealand (Procter et al., 2010), generated a value of 1 m^3/m^2 (total affected area of 7 x 10^6 m^2; erosion of 5 x 10^6 m^3; deposition of 2 x 10^6 m^3). As another example, in a braided river in a natural regime in Scotland (Wheaton et al., 2010), a maximum activity index of 0.17 was estimated over several surveys (total affected area of 1.15 x 10^4 m^2; erosion of 11162 m^3; deposition of 8882 m^3).

Another direct use of DoDs is its capacity to highlight the source of the mobilized sediment. In the study period (2015-16), the reach was fed by a positive net gravel volume of 18,690 m^3. This value is considered the minimum sediment income from upstream –and this is important– since a certain amount of sediment particles may have been transported through our study reach without being stored. This net sediment input to the system, in relative terms, corresponds to

less than 20% of the total deposited sediment and only 10.4% of the total mobilized sediment. Hence, bed and bank erosion, the two main processes identified, were the main source of the sediment (73,803 m^3) that moved along the reach. This agrees with the observations made in Calle et al. (2017), which revealed a continuous exhumation of rocks and older materials 30 years after the discontinuation of intensive in-stream gravel mining. This finding supports a long-term self-adjustment of streams affected by gravel mining, especially as a consequence of the local erosion and remobilization of sediment at the reach scale.

4.2 Sub-reach scale geomorphic interpretations

The previous section described how mobilized volumes provide information on morphodynamics by standard DoD calculations. However, more information can be obtained from a DoD when applying the methodology presented here, i.e. by dividing the DoD into strips (Supplementary material 1) and automatically identifying boundary types (Supplementary material 2). This offered insights into morphologic patterns of change, sub-reach-scale mobilized volumes and ranges of sediment transfer.

4.2.1 Longitudinal patterns of morphological change

The automatic strip division produced 660 strips, 10 m in length, where erosion, deposition and net change (Figure 4**Error! Reference source not found.**-b) can b e calculated individually. Automatic clustering of areas with similar behaviours produced 34 clusters: 17 depositional and 17 erosional (Figure 4**Error! R eference source not found.**-c), which displayed a successive pattern of erosion and deposition couplets. The lengths of these clusters and the mobilized

sediment volumes they contained (Table 2) were far from homogeneous; from 10 to 1050 m in length and 80 to 45867 m^3. Additionally, the sum of only nine clusters from this heterogeneous distribution of cluster lengths and sediment volumes accounted for 75% of the total length of the reach and 81% of the total mobilized sediment volume (namely clusters 2, 3, 12, 25, 27, 28, 32, 33, 34; from up to downstream in Figure 5-b). This pointed to the different behaviour of areas with shorter clusters compared to areas with longer clusters (in the same floods in the study). Longer clusters mobilized the largest amount of sediment, and can be interpreted as an indicator of unbalanced morphosedimentary dynamics and the general adjustment conditions of the river. The highest ratios of sediment volume per unit length (last column in Table 2) are located in the lower reach (between 0 and 2250 m), which, in addition to their length and total volume, is indicative of downstream morphosedimentary instability. We speculate that these segments are related to in-stream mining since these activities were especially intense in this area, as part of the strategy deployed to prevent the siltation of the Maria Cristina reservoir (located 3 km downstream). The rest of the clusters, significantly smaller, are thought to reflect local controls and processes induced by local changes in channel geometry, for example. Figure 4**Error! Reference source not found.**-c shows how these small variations are concentrated between 4500 and 5800 m of the reach and rarely appear elsewhere. These rapid changes could also indicate that transport capacity is close to the threshold, so minor changes in channel geometry are driving the sediment entrainment. We consider that these areas may be somewhat adapted to the new morphosedimentary dynamics.

373 *4.2.2 Sub-reach-scale mobilized volumes: segments*

374 Figure 4**Error! Reference source not found.**-b shows sediment balance and t
375 otal sediment input within each cluster, where cylinders give visual guidance
376 about the spatial distribution of mobilized sediment volumes along the reach.
377 Table 2 also shows the eroded and deposited volume, the net balance (deposits
378 minus erosion) and the total mobilized volume of sediment (deposit plus erosion)
379 for each segment. Both, Figure 4 and Table 2, reveal that the greatest deposition
380 and erosion occurred in the most downstream area of the reach (segments 10
381 and 11), accounting for 45% of the total mobilized volume (see Table 2).

382 *4.2.3 Estimating sediment transfer*

383 The computed strip division shows eighteen depositional boundaries (type #1)
384 along the reach, where the erosive segment exports sediment directly to a
385 downstream depositional segment. Sediment transport calculations from and to
386 these eighteen depositional boundaries provide ranges of sediment transfers
387 (maximum and minimum sediment displacements). The results obtained at
388 boundaries #105, 513, 543, 647 and 659 (marked as with an asterisk (*) in Table
389 3) are of particular interest. In the downstream boundary (#105), the results show
390 a maximum distance of up to 5550 m, which evidences the need of sediment
391 travelling across the entire reach to explain this deposition. At the same
392 boundary, the estimation of the minimum displacement was 2030 m, describing
393 a motion range of 2030 m to over 5550 m. In the case of depositional boundaries
394 #659 and #647, the upstream minimum displacement approach obtained enough
395 transfer distance to explain the upstream sediment input, which in fact constitutes
396 the mathematical evidence of sediment input from the upper limit of the analysed
397 system. A part from previous examples, minimum and maximum sediment

398 mobility ranges were computed at each depositional boundary, and provided
399 information on the variations in these values along the reach (see Table 3).

400 Conversely, when considering the upstream accumulated net erosion and its
401 comparison and balance with downstream deposits, none of the downstream
402 maximum or minimum distances can be seen to attain the outlet of the reach.
403 This means that none of the sediment eroded inside the reach is sufficient to
404 demonstrate mathematically that it is carried through the most downstream strip,
405 i.e. strip no. 0. Eroded sediment is thus always deposited before the downstream
406 limit of the reach (so no asterisk in 'Downstream maximum and minimum'
407 columns of Table 3).

408 *4.2.4 Tracers*

409 Marked particles were used to compare the results of sediment entrainment and
410 the travel distance of discrete gravel and boulder particles with displacements
411 calculated from DoD. The estimated distances and characteristics of tracers that
412 moved more than one strip distance are shown in Table 4. The recovery rate was
413 28%, but only 11% considering stones that were transported over one metre. The
414 marked particles that coincide with erosive segment 6 (see upper yellow lines in
415 **Error! Reference source not found.**-c) rolled downstream 328 m and 162 m, i.e p
416 ebble U62 and U58, with weights of 0.8 and 2 kg respectively. The middle site is
417 located in depositional segment 7, where pebbles M06 and M10 rolled 72 m and
418 59 m, weighing 0.2 and 1 kg respectively. The marked particles located in
419 segment 11 were buried and did not show any movement. These results
420 evidenced, a priori, a good correlation between particle movement and estimated
421 sediment transfers.

4.3 Functional connectivity

In our case study, the connectivity values ($C_{v\text{-}strip}$) from DoD apply to the accumulated effects of two moderate magnitude floods. Figure 5 shows the longitudinal connectivity values (c) and their relationships with deposition, erosion (a), and net volumes (b).

Lower values of $C_{v\text{-}strip}$ (below 1) highlight the strips where deposition predominates, which imply a decrease in connectivity (e.g. segment 11; 0 to 1000 m) due to reduced sediment conveyance further down. It does not mean that it has no transport coming from upstream, it indicates the storage of the mentioned incoming sediment. Conversely, higher values (above 1) highlight the dominance of erosion processes (e.g. in segment 10; 1000 to 2000 m) which indicate that sediment connectivity is increasing given that sediment entrainment is high. Values of about 1 (e.g. segments 5 and 4; 4000 to 6000 m) indicate sediment balance, i.e. erosion and deposition are equal in magnitude.

5 Discussion

5.1 Boundary significance

A morphosedimentary significance can now be added to the boundaries mathematically defined in section 3.2. Boundary types #2 and #4 represent depositional and erosive continuity respectively, and are found in clusters where depositional or erosive processes remain dominant. Type #5 was not found in this study, but its presence may indicate either no change or an equilibrium in the erosion-deposition budget in the river channel (net volume = 0). Type #1 and #3 boundaries signal changes in the river channel behaviour from erosive to

445 depositional conditions or vice versa. Evidence of these boundaries in the field is
446 shown in Figure 6. Boundary type #1, known as a depositional boundary, reveals
447 the most interesting geomorphic relationship since, in the simplest scenario, a
448 direct longitudinal connectivity can be assumed between them. The upstream
449 eroded sediment is most likely to be represented by the downstream deposited
450 sediment. In this sequence, the upstream erosion cluster (exemplified in Figure
451 3) concentrates flow and produces an excess of energy that enhances banks and
452 riverbed erosion. This may be exacerbated in streams affected by gravel mining,
453 as they previously had the condition of hungry waters (Kondolf, 1997).
454 Downstream, as the flow loses confinement, the channel becomes a depositional
455 cluster where previously eroded sediments are most likely to be deposited (see
456 field examples of Figure 6).

457 In contrast, boundary type #3 (erosive boundary) represents a change in
458 behaviour from a depositional to an erosive channel, as the streamflow loses
459 transport capacity and sediment load. Two different types of erosional boundaries
460 have been identified. The first is a situation where boundary limit #3 does not
461 imply a disruption in sediment continuity (e.g. Figure 6-c). These conditions are
462 evidence of a highly functional downstream connectivity. The second is a
463 configuration where this boundary is also accompanied by scarce or null
464 sediment continuity (Figure 6-b), and is clearly indicative of a lack of functional
465 connectivity due to sediment scarcity. The latter case corresponds to highly
466 altered reaches where the sediment wave advances towards geomorphic “dead”
467 areas in a naturally-induced recovery process. The ultimate field representation
468 of this is the lobe-shaped bars described in Calle et al. (2015), also well
469 represented in Figure 6.

The pattern changes in boundary types #1 and #3 is what this method highlights the most effectively. We believe this to be a particularly useful finding in view of the fact that these behavioural changes are not usually very evident in field observations and it is particularly difficult to draw lines between reaches with different morphosedimentary behaviour through a traditional geomorphological map.

5.2 Sediment motion and connectivity

The spatial pattern of morphological change is related to bedload transport (Ferguson et al., 1992). Consequently, we used a DoD, the ultimate expression of change, to estimate the transfer of sediment between erosion and deposition sites. Nevertheless, the limitations of this technique should be noted. DoD analysis cannot track individual bed particles; it detects the surface changes, regardless of particle size, from which a range of sediment motion can be derived. Further field texture sampling of the active area is what gives an idea of the size of the sediment associated with this movement. Sediment transfers are calculated based on the simplest and least energetic explanation for moving bulk sediment, but may also include several steps separated by rest periods during a single event or events. After considering these assumptions, a comparison with the other estimated parameters is possible.

According to the results, a high connectivity value, such as the ones associated with segments 6 or 10, is related to the highest downstream estimated transport distances, highest eroded volumes and long erosive clusters. These conditions match a generalized low level of sediment availability, high transport distances and therefore less sediment retention. Lowest connectivity values, e.g. segments

494 9 and 11, are related to high upstream transport distances, highest deposited
495 volumes and longest depositional clusters, and therefore high level of sediment
496 retention. These high or low $C_{v\text{-}strip}$ values predominates in the lower segments of
497 the reach (Figure 5-a), which has the highest amounts of erosion, deposition,
498 transport distances and abrupt changes in connectivity. On the contrary, $C_{v\text{-}strip}$
499 values close to 1, e.g. segments 3, 4 and 5, coincide with alternating erosive-
500 depositional clusters, low volumes and short clusters that suggest short-duration
501 particle motions, dynamic stability, a close threshold of entrainment of the bed
502 material, and a certain level of recovery (compared to segments 9-11).

503 This also correlates well with the tracer transport distance, although these are
504 discrete data. Estimated transport distances are fairly close to the recorded tracer
505 transport, e.g. 310 m recorded on a marked 64 mm gravel particle and from 10
506 m to 230 and 370 m estimated with downstream minimum displacement for the
507 boundaries 443-485 (see Figure 4**Error! Reference source not found.** and T
508 able 3). However, tracers located in the middle and lower sites had lower
509 transport rates or even no transport. This contrasts with increasing path length
510 values calculated further downstream, and could be due to the following main
511 reasons: i) not enough pebbles have been set for the experiment; ii) pebbles that
512 experienced longer transport distances were not found after the flood; iii) pebble
513 movement in depositional clusters does not reflect actual step lengths (Figure 7-
514 a and -b); iv) the calculated transport lengths are a measure of bulk sediment
515 displacement that cannot be compared to individual step lengths; and v) the
516 recovered pebbles had a D50 of 64 mm and active bars had a D50 of 22.6 mm.
517 Hitherto, no objective reason can be selected and more experiments should be

518 carried out to determine the reason for this difference on estimated transport
519 distances.

520 5.3 Discussion of the applicability of the method

521 5.4 Implications for river management in Mediterranean regions

522 Within the European Framework Directive, the sources, transfer and retention of
523 sediment have become a focus of research for river management and restoration
524 in many Mediterranean rivers (Nikolaidis et al., 2013; Sanchis-Ibor et al., 2017,
525 among others). A broad understanding of ephemeral river dynamics can be
526 achieved by combining DEMs and the methodology presented here. In this
527 context, where estimation of hydrological, biological and physico-chemical water
528 parameters usually fails, connectivity may serve as a basis for assessing fluvial
529 resilience to perturbation, applied to management strategies (Bizzi et al., 2016).
530 Our findings suggest that short erosive-depositional strip clusters (< 400 m,
531 according to Figure 5-b) and short step lengths are indicative of sediment
532 restoration, geomorphic diversity and river recovery. In practical terms, river
533 segments with connectivity values close to 1 show a positive recovery and
534 balance of morpho-sedimentary dynamics. Conversely, a high connectivity value
535 denotes highly perturbed conditions which, in the case of sediment-starved
536 reaches, may have important consequences in terms of potential geomorphic
537 recovery over human time scales (Brooks and Brierley, 2004).

538 In-stream aggregate mining is one of the most common human perturbations
539 carried out on rivers worldwide. In Mediterranean regions, it was used to prevent
540 sediment siltation in reservoirs, as a flood prevention practice, and as a source

of aggregate material for the construction sector. These mining activities have led to environmental problems and geomorphological disruptions with impacts on sediment load and channel geometry (Kondolf, 1997; Hooke, 2006; Downs et al., 2013; Calle et al., 2017; Sanchis-Ibor et al., 2017). Aggregate extraction produces sediment exhaustion, gravel bed compaction and a decrease in hydraulic roughness, among other phenomena, affecting river landform development, sediment transport and connectivity (Hooke, 2006). Our findings pointed out that the role of in-stream mining was critical in increasing sediment yields downstream from reworked alluvium. In those sites, the increased flow competence through channel incision, lead to coupling the longitudinal channel components (Fryirs and Brierley, 1999) which suffers the next decoupling due to subsequent intense deposition and formation of lobe-shaped bars (Figure 6, black dashed line). These bars are diagnostic landforms of altered rivers by gravel mining (Figure 5; Calle et al., 2015) and were also described in eastern Spain by Sanchis-Ibor et al. (2017), in southern Spain by Hooke (2003), and in other Mediterranean rivers (Calle et al., 2017). The methodology presented here can automatically detect these features, which have been redefined in this paper as ‘depositional boundaries’. The potential of this method lies precisely in the automatic identification of these diagnostic features that can be now used to detect sediment-related environmental problems in any river system where a DoD is obtained.

6 Conclusions

In this paper, we propose a reproducible and automated method for analysing repeat topographic models of river channels, which focuses on to the

565 geomorphological interpretation of a DoD. The described method allows
566 objectively to infer i) the spatial pattern of morphological change, ii) the sediment
567 transfer volumes and distances, and iii) the functional sediment connectivity.

568 This new approach of understanding outputs of DoD applied to the example of
569 Rambla de la Viuda has resulted in a deep understanding of the geomorphic
570 processes acting in the studied reach. Bed and bank erosion were pointed out to
571 be the main source of sediment contributing to a self-adjustment of the reach
572 exerting a positive influence on morphologic reactivation and short-term river
573 recovery. Further analysis discovered and mapped a sequence of coupled
574 erosion-deposition segments (clusters) at reach scale. The length and sediment
575 volume of these sequences is sensitive to the channel dynamic equilibrium.
576 Larger clusters (>400 m) occurred in areas of historically intense mining and a
577 higher degree of instability. Shorter clusters denoted proximity to the transport
578 threshold and thus a higher degree of morphodynamic balance or geomorphic
579 recovery.

580 Estimation of sediment transfers and transport distances is an additional tool that
581 helps understanding the reach scale sources and sinks of sediment that this
582 method provides. The method used a longitudinal strip division of the studied
583 reach to estimate maximum (a) and minimum (b) transport from upstream (1) and
584 to downstream (2) of key boundaries (Type#1). The range of sediment transfer
585 based on DoD maps, together with the presented method, was found to correlate
586 well with surveyed travel distances from tracers located in erosive clusters, i.e.
587 maintained erosive conditions. Conversely, the estimated displacements of
588 tracers allocated on depositional segments did not match most likely due to

589 buried tracers. In this sense, additional tracer information, by adding more
590 frequent tracer stations or new recovery method, would increase validation of the
591 model over the whole studied reach.

592 Functional sediment connectivity ($C_{v\text{-}strip}$) was estimated as the ratio between the
593 sediment exported (erosion) and retained (deposition) in each channel strip (10
594 m in length). High longitudinal connectivity was associated with long erosive
595 clusters and low longitudinal connectivity to long depositional clusters. Higher and
596 lower values of connectivity were found associated with sediment disruptions
597 caused by mining, in our case at the downstream reach. Balanced values of
598 erosion and deposition gave $C_{v\text{-}strip}$ values close to 1. These values are
599 associated with shorter clusters, indicating a certain degree of adjustment or a
600 dynamic equilibrium of channel conditions.

601 From an environmental perspective, the degree of sediment connectivity strongly
602 influences the system geomorphic resilience to natural (e.g. floods) and human-
603 induced disturbances (e.g. land use change or instream mining). This new
604 method of understanding DoD will contribute to: i) a more effective interpretation
605 of morphosedimentary dynamics and connectivity, ii) increase river behavioural
606 predictability (Hooke and Mant, 2002), iii) improve the quantification of its
607 environmental state (Wohl, 2017), and iv) also help to establish acceptable
608 geomorphic recovery targets that may contribute to implement realistic and
609 sustainable river rehabilitation practices from an hydromorphological point of view
610 in the framework of the EU Water Directive.

7 Acknowledgements

We would like to thanks the constructive criticism received by an unknown reviewer, the Associate Editor, and especially to Richard Williams for his final reviews and support. We also thanks JoJo Mangano for the English support. This paper was funded by the Ministry of Science, Innovation and Universities through the project “Improvements in sedimentary and hydrologic response to environmental and climatic changes in Mediterranean watersheds” (CGL2014-58127-C3-1-R) and “Assessment and modelling eco-hydrological and sedimentary responses in Mediterranean catchments for climate and environmental change adaptation” EPHIMED (CGL2017-86839-C3-1-R). MC was funded by the Spanish FPI scholarship (BES-2012-056723), JC developed the full code for estimating step lengths and actively helped resolve conceptual transport issues. PA received funding from the Academy of Finland, the Strategic Research Council (COMBAT project, Grant 293389). Special thanks go to Alicia Castán for providing field support during flights. The authors declare no conflict of interest.

8 References

Alho, P., Kukko, A., Hyyppä, H., Kaartinen, H., Hyyppä, J., Jaakkola, A., 2009. Application of boat-based laser scanning for river survey. Earth Surface Processes and Landforms, 34(13), 1831-1838.

Alho, P., Vaaja, M., Kukko, A., Kasvi, E., Kurkela, M., Hyyppä, J., Hyyppä, H., Kaartinen, H., 2011. Mobile laser scanning in fluvial geomorphology: mapping and change detection of point bars. Zeitschrift f??r Geomorphologie, Supplementary Issues, 55(2), 31-50.

Anadón, P., Moissenet, E., 1996. Neogene basins in the Eastern Iberian Range. In: C.J. Dabrio, P.F. Friend (Eds.), Tertiary Basins of Spain: The Stratigraphic Record of Crustal Kinematics. World and Regional Geology. Cambridge University Press, Cambridge, pp. 68-76.

Antoniazza, G., Bakker, M., Lane, S.N., 2019. Revisiting the morphological method in two-dimensions to quantify bed-material transport in braided rivers. Earth Surface Processes and Landforms, 44(11), 2251-2267.

639 Bizzi, S., Demarchi, L., Grabowski, R.C., Weissteiner, C.J., Van de Bund, W., 2016. The use of remote
640 sensing to characterise hydromorphological properties of European rivers. Aquatic Sciences,
641 78(1), 57-70.

642 Bracken, L.J., Croke, J., 2007. The concept of hydrological connectivity and its contribution to
643 understanding runoff-dominated geomorphic systems. Hydrological Processes, 21(13), 1749-
644 1763.

645 Bracken, L.J., Turnbull, L., Wainwright, J., Bogaart, P., 2015. Sediment connectivity: a framework for
646 understanding sediment transfer at multiple scales. Earth Surface Processes and Landforms, 40(2),
647 177-188.

648 Brasington, J., Langham, J., Rumsby, B., 2003. Methodological sensitivity of morphometric estimates of
649 coarse fluvial sediment transport. Geomorphology, 53(3–4), 299-316.

650 Brasington, J., Vericat, D., Rychkov, I., 2012. Modeling river bed morphology, roughness, and surface
651 sedimentology using high resolution terrestrial laser scanning. Water Resources Research, 48(11),
652 W11519.

653 Brooks, A.P., Brierley, G.J., 2004. Framing realistic river rehabilitation targets in light of altered sediment
654 supply and transport relationships: Lessons from East Gippsland, Australia. Geomorphology,
655 58(1-4), 107-123.

656 Calle, M., Alho, P., Benito, G., 2017. Channel dynamics and geomorphic resilience in an ephemeral
657 Mediterranean river affected by gravel mining. Geomorphology, 285, 333-346.

658 Calle, M., Alho, P., Benito, G., 2018. Monitoring ephemeral river changes during floods with SfM
659 photogrammetry. Journal of Iberian Geology, 44(3), 355-373.

660 Calle, M., Lotsari, E., Kukko, A., Alho, P., Kaartinen, H., Rodriguez-Lloveras, X., Benito, G., 2015.
661 Morphodynamics of an ephemeral gravel-bed stream combining Mobile Laser Scanner, hydraulic
662 simulations and geomorphological indicators. Zeitschrift für Geomorphologie, Supplementbände,
663 59(3), 33-57.

664 Camarasa-Belmonte, A.M., Segura-Beltrán, F., 2001. LAS CRECIDAS EN RAMBLAS VALENCIANAS
665 MEDITERRÁNEAS. Estudios Geográficos, 62, 245.

666 Cavalli, M., Trevisani, S., Comiti, F., Marchi, L., 2013. Geomorphometric assessment of spatial sediment
667 connectivity in small Alpine catchments. Geomorphology, 188, 31-41.

668 Crema, S., Cavalli, M., 2018. SedInConnect: a stand-alone, free and open source tool for the assessment of
669 sediment connectivity. Computers & Geosciences, 111, 39-45.

670 Downs, P.W., Dusterhoff, S.R., Sears, W.A., 2013. Reach-scale channel sensitivity to multiple human
671 activities and natural events: Lower Santa Clara River, California, USA. Geomorphology, 189,
672 121-134.

673 Eltner, A., Kaiser, A., Abellan, A., Schindewolf, M., 2017. Time lapse structure-from-motion
674 photogrammetry for continuous geomorphic monitoring. Earth Surface Processes and Landforms,
675 n/a-n/a.

676 Ferguson, R.I., Ashmore, P.E., Ashworth, P.J., Paola, C., Prestegaard, K.L., 1992. Measurements in a
677 Braided River chute and lobe: 1. Flow pattern, sediment transport, and channel change. Water
678 Resources Research, 28(7), 1877-1886.

679 Flener, C., Vaaja, M., Jaakkola, A., Krooks, A., Kaartinen, H., Kukko, A., Kasvi, E., Hyyppä, H., Hyyppä,
680 J., Alho, P., 2013. Seamless Mapping of River Channels at High Resolution Using Mobile LiDAR
681 and UAV-Photography. Remote Sensing, 5(12), 6382-6407.

682 Fryirs, K., 2013. (Dis)Connectivity in catchment sediment cascades: a fresh look at the sediment delivery
683 problem. Earth Surface Processes and Landforms, 38(1), 30-46.

684 Fryirs, K., Brierley, G.J., 1999. Slope–channel decoupling in Wolumla catchment, New South Wales,
685 Australia: the changing nature of sediment sources following European settlement. CATENA,
686 35(1), 41-63.

687 Fryirs, K.A., Brierley, G.J., Preston, N.J., Kasai, M., 2007. Buffers, barriers and blankets: The
688 (dis)connectivity of catchment-scale sediment cascades. CATENA, 70(1), 49-67.

689 Goff, J.R., Ashmore, P., 1994. Gravel transport and morphological change in braided sunwapta river,
690 Alberta, Canada. Earth Surface Processes and Landforms, 19(3), 195-212.

691 Heckmann, T., Vericat, D., 2018. Computing spatially distributed sediment delivery ratios: inferring
692 functional sediment connectivity from repeat high-resolution digital elevation models. Earth
693 Surface Processes and Landforms.

694 Hodge, R., Brasington, J., Richards, K., 2009a. Analysing laser-scanned digital terrain models of gravel
695 bed surfaces: linking morphology to sediment transport processes and hydraulics. Sedimentology,
696 56(7), 2024-2043.

697 Hodge, R., Brasington, J., Richards, K., 2009b. In situ characterization of grain-scale fluvial morphology
698 using Terrestrial Laser Scanning. Earth Surface Processes and Landforms, 34(7), 954-968.

699 Hooke, J., 2003. Coarse sediment connectivity in river channel systems: a conceptual framework and
700 methodology. Geomorphology, 56(1–2), 79-94.

701 Hooke, J.M., 2006. Human impacts on fluvial systems in the Mediterranean region. Geomorphology, 79(3),
702 311-335.

703 Hooke, J.M., Mant, J., 2002. Floodwater use and management strategies in valleys of southeast Spain. Land
704 Degradation & Development, 13(2), 165-175.

705 Huang, H., Ding, M., 2016. Linking Functional Connectivity and Structural Connectivity Quantitatively:
706 A Comparison of Methods. Brain Connectivity, 6(2), 99-108.

707 Jaud, M., Passot, S., Le Bivic, R., Delacourt, C., Grandjean, P., Le Dantec, N., 2016. Assessing the accuracy
708 of high resolution digital surface models computed by PhotoScan® and MicMac® in sub-optimal
709 survey conditions. Remote Sensing, 8(6).

710 Javernick, L., Brasington, J., Caruso, B., 2014. Modeling the topography of shallow braided rivers using
711 Structure-from-Motion photogrammetry. Geomorphology, 213, 166-182.

712 Kasvi, E., Vaaja, M., Alho, P., Hyyppä, H., Hyyppä, J., Kaartinen, H., Kukko, A., 2013. Morphological
713 changes on meander point bars associated with flow structure at different discharges. Earth Surface
714 Processes and Landforms, 38(6), 577-590.

715 Kondolf, G.M., 1997. PROFILE: Hungry Water: Effects of Dams and Gravel Mining on River Channels.
716 Environmental Management, 21(4), 533-551.

717 Kondolf, G.M., Boulton, A.J., O'Daniel, S., Poole, G.C., Rahel, F.J., Stanley, E.H., Wohl, E., Bång, A.,
718 Carlstrom, J., Cristoni, C., Huber, H., Koljonen, S., Louhi, P., Nakamura, K., 2006. Process-based
719 ecological river restoration: Visualizing three-dimensional connectivity and dynamic vectors to
720 recover lost linkages. Ecology and Society, 11(2).

721 Lane, S.N., Reid, S.C., Westaway, R.M., Hicks, D.M., 2005. Remotely Sensed Topographic Data for River
722 Channel Research: The Identification, Explanation and Management of Error, Spatial Modelling
723 of the Terrestrial Environment. John Wiley & Sons, Ltd, pp. 113-136.

Lane, S.N., Westaway, R.M., Murray Hicks, D., 2003. Estimation of erosion and deposition volumes in a large, gravel-bed, braided river using synoptic remote sensing. Earth Surface Processes and Landforms, 28(3), 249-271.

Lehotský, M., Rusnák, M., Kidová, A., Dudžák, J., 2018. Multitemporal assessment of coarse sediment connectivity along a braided-wandering river. Land Degradation & Development.

Lisle, T.E., Cui, Y., Parker, G., Pizzuto, J.E., Dodd, A.M., 2001. The dominance of dispersion in the evolution of bed material waves in gravel-bed rivers. Earth Surface Processes and Landforms, 26(13), 1409-1420.

Lotsari, E., Vaaja, M., Flener, C., Kaartinen, H., Kukko, A., Kasvi, E., Hyyppä, H., Hyyppä, J., Alho, P., 2014. Annual bank and point bar morphodynamics of a meandering river determined by high-accuracy multitemporal laser scanning and flow data. Water Resources Research, 50(7), 5532-5559.

Machado, M.J., Medialdea, A., Calle, M., Rico, M.T., Sánchez-Moya, Y., Sopeña, A., Benito, G., 2017. Historical palaeohydrology and landscape resilience of a Mediterranean rambla (Castellón, NE Spain): Floods and people. Quaternary Science Reviews, 171, 182-198.

Nikolaidis, N.P., Demetropoulou, L., Froebrich, J., Jacobs, C., Gallart, F., Prat, N., Porto, A.L., Campana, C., Papadoulakis, V., Skoulikidis, N., Davy, T., Bidoglio, G., Bouraoui, F., Kirkby, M., Tournoud, M.-G., Polesello, S., Barberá, G.G., Cooper, D., Gomez, R., Sánchez-Montoya, M.d.M., Latron, J., De Girolamo, A.M., Perrin, J.-L., 2013. Towards sustainable management of Mediterranean river basins: policy recommendations on management aspects of temporary streams. Water Policy, 15(5), 830-849.

Procter, J.N., Cronin, S.J., Fuller, I.C., Lube, G., Manville, V., 2010. Quantifying the geomorphic impacts of a lake-breakout lahar, Mount Ruapehu, New Zealand. Geology, 38(1), 67-70.

Sanchis-Ibor, C., Segura-Beltrán, F., Almonacid-Caballer, J., 2017. Channel forms recovery in an ephemeral river after gravel mining (Palancia River, Eastern Spain). CATENA, 158, 357-370.

Simón, J.L., Pérez-Cueva, A.J., Calvo-Cases, A., 2013. Tectonic beheading of fluvial valleys in the Maestrat grabens (eastern Spain): Insights into slip rates of Pleistocene extensional faults. Tectonophysics, 593(0), 73-84.

Snavely, K.N., 2009. Scene reconstruction and visualization from internet photo collections, University of Washington, 169 pp.

Verhoeven, G., 2011. Taking computer vision aloft – archaeological three-dimensional reconstructions from aerial photographs with photoscan. Archaeological Prospection, 18(1), 67-73.

Verhoeven, G., Doneus, N., Doneus, M., Štuhec, S., 2015. From pixel to mesh: accurate and straightforward 3D documentation of cultural heritage from the Cres/Lošinj archipelago, Istraživanja na otocima. Hrvatsko arheološko društvo-Lošinjski muzej, pp. 165-176.

Vericat, D., Wheaton Joseph, M., Brasington, J., 2017. Revisiting the Morphological Approach. Gravel-Bed Rivers.

Wang, Y., Liang, X., Flener, C., Kukko, A., Kaartinen, H., Kurkela, M., Vaaja, M., Hyyppä, H., Alho, P., 2013. 3D Modeling of Coarse Fluvial Sediments Based on Mobile Laser Scanning Data. Remote Sensing, 5(9), 4571-4592.

Wester, T., Wasklewicz, T., Staley, D., 2014. Functional and structural connectivity within a recently burned drainage basin. Geomorphology, 206, 362-373.

Westoby, M.J., Brasington, J., Glasser, N.F., Hambrey, M.J., Reynolds, J.M., 2012. 'Structure-from-Motion' photogrammetry: A low-cost, effective tool for geoscience applications. Geomorphology, 179, 300-314.

769 Wheaton, J.M., Brasington, J., Darby, S.E., Sear, D.A., 2010. Accounting for uncertainty in DEMs from
770 repeat topographic surveys: improved sediment budgets. Earth Surface Processes and Landforms,
771 35(2), 136-156.

772 Wohl, E., 2017. Connectivity in rivers. Progress in Physical Geography, 41(3), 345-362.

773 Wolman, M.G., 1954. A method of sampling coarse river-bed material. American Geophysical Union.

774

775

776 **Table 1: Summary of photogrammetric survey characteristics. 'Overlap' is the mean number of**
777 **projections of points. 'N. of targets' refers to the number of targets used for the topographic**
778 **reconstruction and 'Target type' to mobile targets (M) and fixed targets (F). Further information may**
779 **be accessed in the photogrammetric reconstruction table of the supplementary information and in**
780 **Calle et al. (2018).**

Fight	Nominal flight height (m)	Sensor	Sensor Size (mm)	Camera res. (pix)	Focal length (mm)	Overlap	N. of targets	Target type	Point-cloud density (pts/m^2)	DEM resolution (cm/px)
F-1	120	Cannon PowerShot G9	7.6 x 5.7	4000x 3000	7.4	21	143	M	515.8	5.58
F-3	75 and 150	Nikon D5500	23.5 x 15.6	6000x 4000	18-36	29	138+ 67	M+ F	1295.4	3.11

781

782 **Table 2: Total volume and mobilized volumes at clusters.**

Segment	Number of clusters	Segment length (m)	Deposition (m^3)	Erosion (m^3)	Net volume (m^3)	Total mobilized volume (m^3)
1	1	120	1083	-2924	-1841	4007
2	1	330	8518	-4581	3937	13098
3	5	450	1903	-4173	-2270	6076
4	7	690	7566	-2987	4579	10552
5	10	680	2373	-5166	-2793	7538
6	3	1360	2090	-14501	-12411	16591
7	3	740	10206	-4257	5948	14463
8	2	140	3729	-7849	-4120	11578
9	1	200	7610	-1040	6569	8650
10	1	830	6466	-21409	-14943	27874
11	1	1050	40950	-4917	36033	45867
Total	**34**	**6590**	**92493**	**-73803**	**18690**	**166296**

783

784

785 **Table 3: Estimated maximum and minimum displacements at type #1 boundaries. Boundaries are**
786 **numbered from downstream (0) to upstream (660) according to the direction of movement in the**
787 **code calculations. Upstream maximum displacement: theory 1a. Downstream maximum**
788 **displacement: theory 2a. Upstream minimum displacement: theory 1b. Downstream minimum**
789 **displacement: theory 2b.**

Boundary (#)	Upstream maximum displacement (m)	Downstream maximum displacement (m)	Upstream minimum displacement (m)	Downstream minimum displacement (m)
647	*130	170	*130	80
576	10	480	10	360
573	10	90	10	10
569	90	50	40	20
554	250	60	50	20
543	*1170	20	520	10
513	*1470	40	280	30
485	20	4470	20	370
455	10	4150	10	230
452	10	4110	10	10
437	20	3960	10	230
433	60	10	10	10
366	20	3240	10	930
296	500	2490	470	670
223	20	250	10	10
208	1550	100	100	90
105	*5550	570	2030	500
Mean	605	207	1366	201

790

791

Table 4: Table with the tracer results showing only the pebbles that were transported more than one strip (~10 m). The upstream site is represented with the letter "U", and the middle site with "M". None of the particles in the most downstream segment were displaced and are therefore not displayed in this table.

Code	Displacement (m)	Strips	Weight (g)	Axes (cm)			Sieve (mm)
				a	b	c	
U31	22.9	2	520	10.1	8.9	4.2	64
U67	31.7	3	1137	11.2	9.6	7.4	64
U62	328.5	31	847	10.2	9.6	6.9	64
U58	162.7	17	2020	13.2	11.2	9.5	90
M21	11.6	1	1518	13.4	11.5	6.4	90
M24	12.2	1	1551	11.7	10.8	7.4	90
M08	13.9	1	2226	14.7	12.6	8.4	90
M16	23.5	2	273	7.3	6.0	5.0	45
M01	33.3	3	362	8.1	7.6	4.5	45
M70	52.9	6	215	8.0	6.1	3.9	45
M10	59.4	6	1091	12.3	10.1	7.4	64
M06	72.6	7	246	8.2	5.9	3.5	45

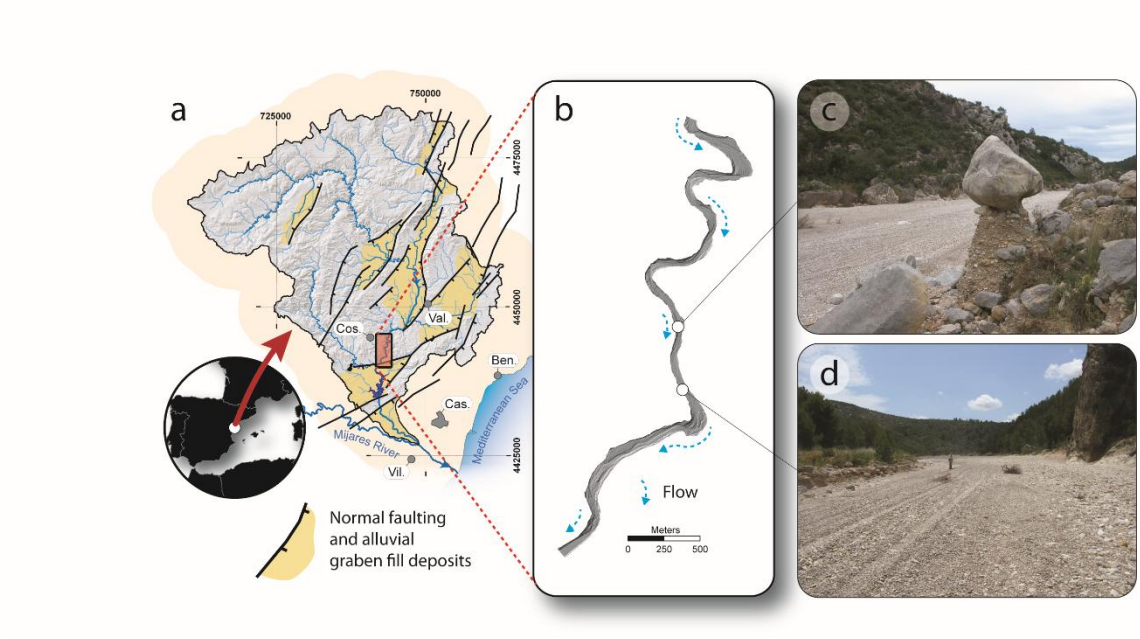

Figure 1: Rambla de la Viuda River in the European and watershed contexts (a) and reach context (b). The figure on the right shows two examples of erosive (c) and depositional (c) areas in the field. The labels of the main towns correspond to Castellón (Cas.), Vall d'Alba (Val.), Costur (Cos.), Villarreal (Vil.) and Benicasim (Ben.).

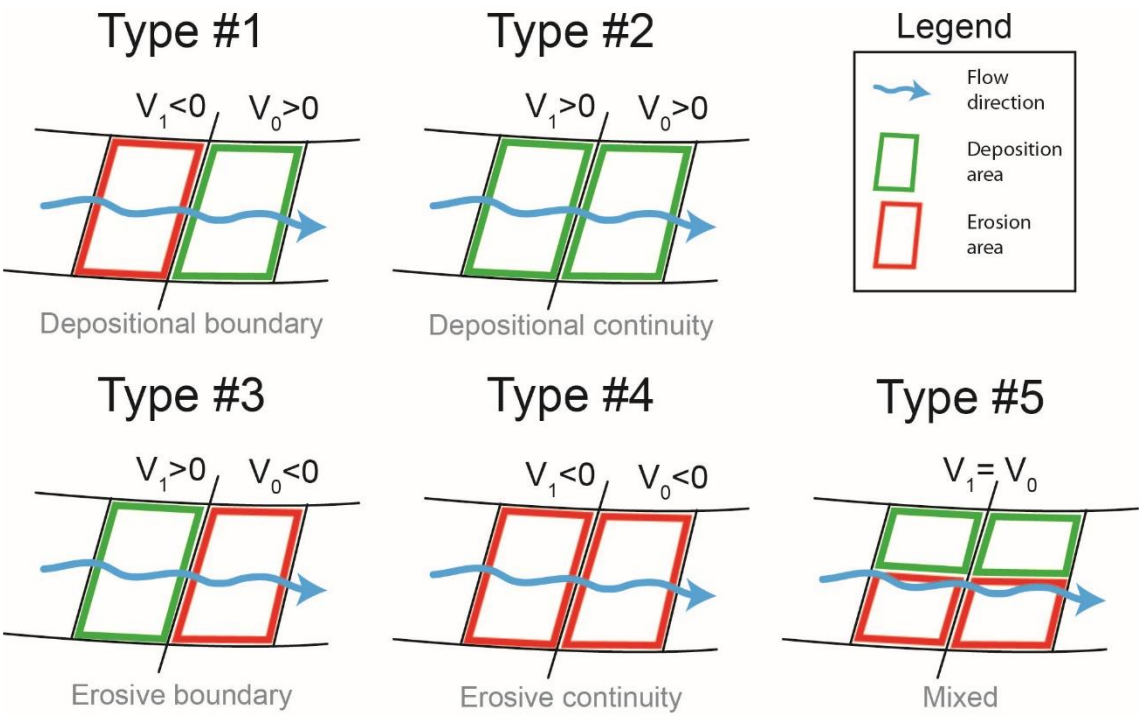

Figure 2: Conceptual boundary definition and types. "V_x" denotes estimated volume from DoD calculations. Boundary type #1: V0>0 and V1<0 (depositional boundary): upstream erosion and downstream deposition; type #2: V0>0 and V1>0 (depositional continuity): upstream deposition and downstream deposition; boundary type #3: V0<0 and V1>0 (erosive boundary): upstream deposition

and downstream erosion; boundary type #4: V0<0 and V1<0 (erosive continuity): upstream erosion and downstream erosion; and a hypothetical type #5 boundary: V0=V1 (balanced limit) was found: net volumes are balanced or close to 0 both upstream and downstream.

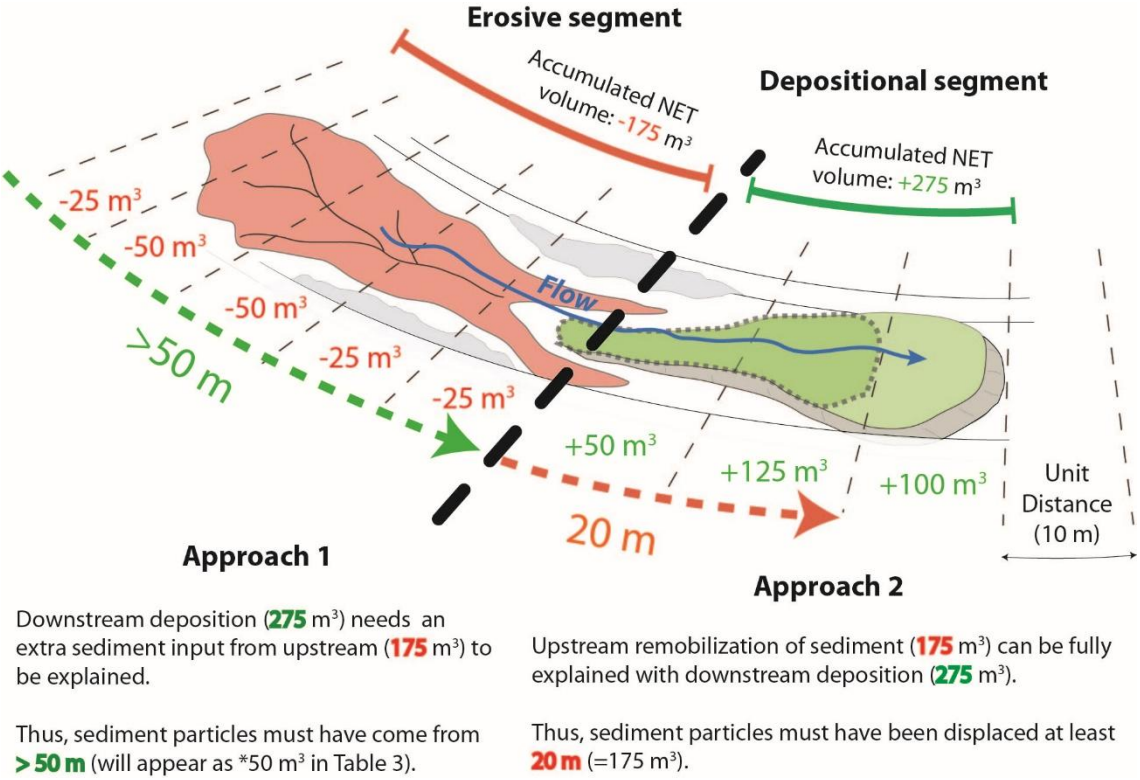

Figure 3: (A) example of path length calculations at depositional boundaries (type #1).

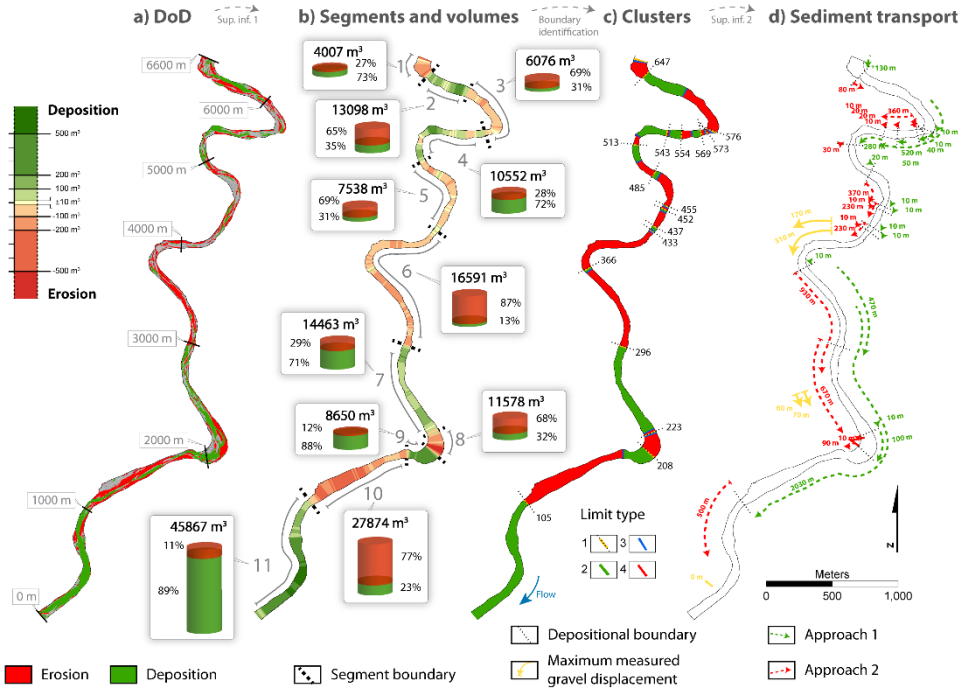

814 **Figure 4: a) Spatial pattern of morphological change (erosion and deposition areas) obtained from**
815 **DoD. b) Strip segmentation results with the net volumes of each segment, proposed segments and**
816 **sediment volumes (cylinders). c) Clustering and boundary type definition. d) Results of approach 1b**
817 **and 2b, i.e. minimum estimated travel lengths. Note that the yellow lines show displacements**
818 **measurd with tracers.**

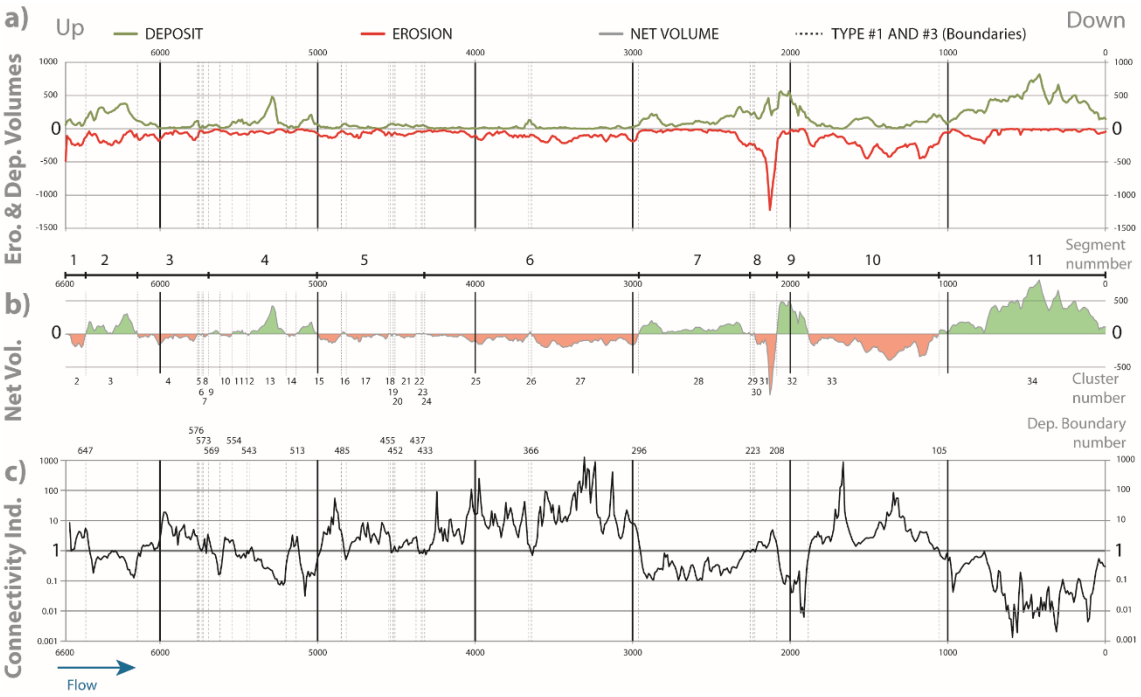

819

820 **Figure 5: a) Deposited and eroded volume b) net volume and c) connectivity value ($C_{v\text{-}strip}$) across**
821 **the reach plotted in a logarithmic scale. Dotted lines divide the 34 clusters and correspond to**
822 **boundary #1 and #3.**

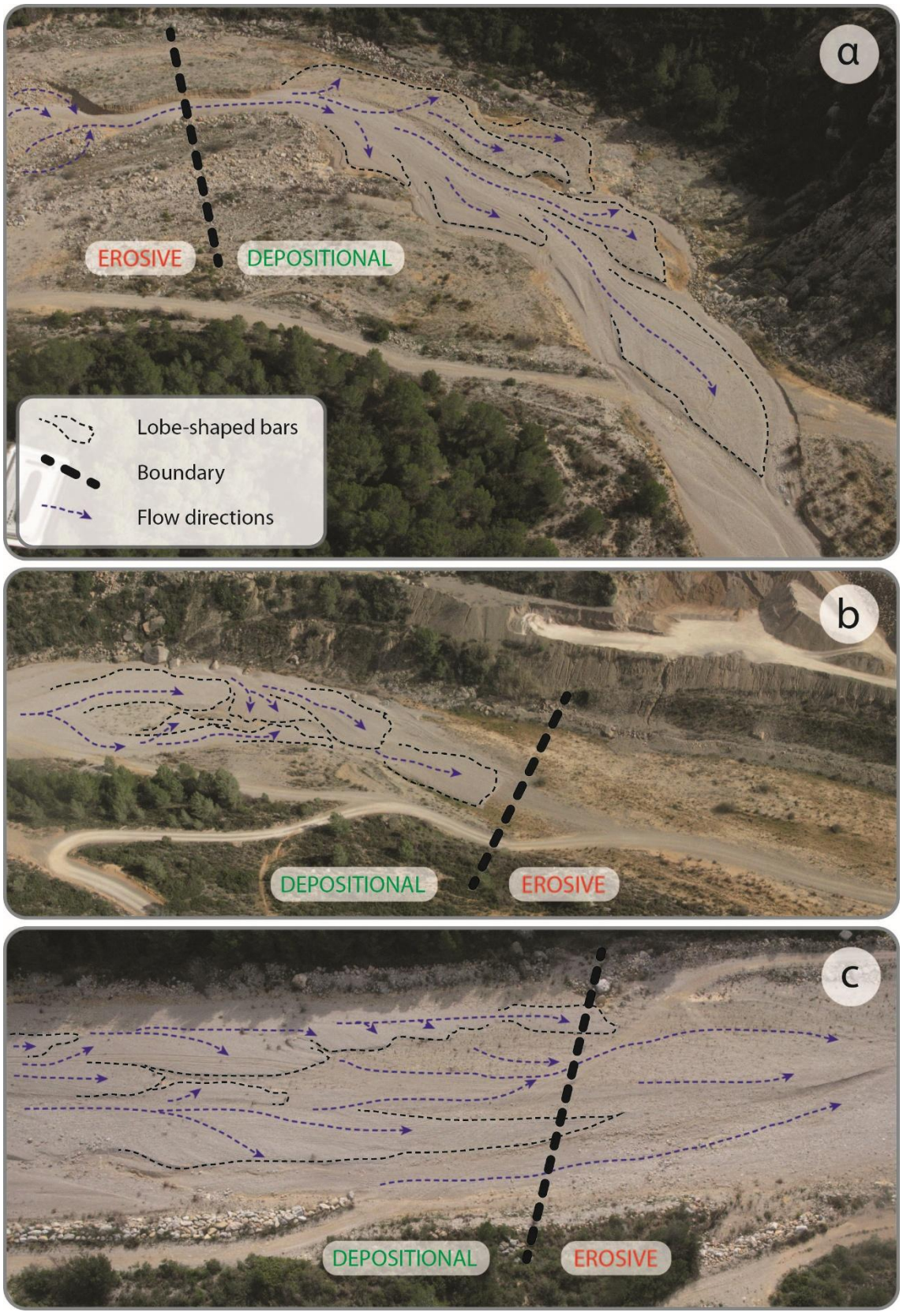

Figure 6: Boundary type #1 (a) and #3 (b and c). The middle and lower pictures show the differences between type #3 with no sediment continuity (b) and sediment continuity (c) indicating different states of sediment connectivity. Flow is always from left to right.

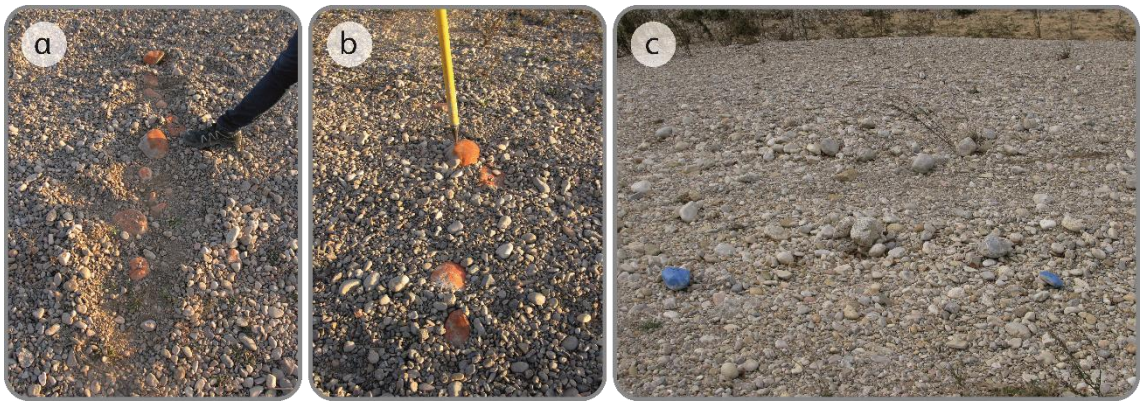

827

828 **Figure 7: Example of pebbles used as tracers for the analysis. They are shown in depositional**

829 **segment 11 (a and b) and erosive segment 6 (c).**

830